Scanning Microscopy Vol. 11, 1997 (Pages 43-52) 0891-7035/97$5.00+.25
Scanning Microscopy International, Chicago (AMF O'Hare), IL 60666 USA

THE INTERPRETATION OF PTYCHOGRAPHICAL RECONSTRUCTIONS FROM SPHALERITE STRUCTURES

T. Plamann

Centre d'Etudes de Chimie Métallurgique CNRS, 94407 Vitry-sur-Seine, France

Abstract

Ptychography is an electron diffraction technique in which Bragg reflections are interfered coherently in order to measure the phases of diffraction orders directly. Two simple reconstruction methods exist, which require different degrees of coherence in the illuminating electron beam. Simulations on InP <110> for two electron accelerating voltages suggest that the asymmetric 'dumbbells' can be reconstructed for small thicknesses, but that the reconstruction methods break down at thicknesses around 10 nm. At larger thicknesses one reconstruction method yields images which show the phosphorus atom. The phase object approximation is shown to break down at thicknesses of about 3.3 nm.

Key Words: Ptychography, sphalerite, super-resolution imaging, phase retrieval, phase object approximation, scanning transmission electron microscopy.

*Address for correspondence:
T. Plamann
Centre d'Etudes de Chimie Métallurgique CNRS,
15 rue Georges Urbain, 94407 Vitry-sur-Seine, France
Telephone number: +33-1-46873593
FAX number:+33-1-46750433
E-mail: plamann@glvt-cnrs.fr

Introduction

Much research is currently being done to extract the phase information in electron microscope images and to reconstruct the electron wavefunction at the exit surface of the specimen in amplitude and phase. A project funded by the European Community was set up, which aimed at the recovery of structural information at 0.1 nm resolution using holography (Lichte, 1992) and focus variation (Coene *et al*., 1992; Van Dyck *et al*., 1993). A different class of image reconstruction methods, comprising tilt series in the conventional high-resolution transmission electron microscope (HRTEM) (Kirkland *et al*., 1995) and super-resolution imaging in the scanning transmission electron microscope (STEM) (Rodenburg and Bates, 1992) are currently being developed in Cambridge, the latter method being the subject of this paper. Although these advances are being made in the quantitative analysis of image contrast, the interpretation of the new information in terms of specimen structure remains somewhat limited. This paper is concerned with the discussion of the limitations and the opportunities of super-resolution imaging in STEM as these are determined by the dynamical interaction of the electron wave with the potential distribution in the local environment of atoms. Throughout the paper, the assumption of a perfect crystal structure will be made, in which case super-resolution imaging is a straightforward extension to a technique called "ptychography" which was introduced by Hoppe (1969a, 1969b, 1982) as a means of measuring the phases of diffraction orders directly.

Nellist *et al*. (1995) showed that Si in the <110> orientation with its dumbbell features can be comfortably reconstructed at a resolution of 0.136 nm using ptychography on data recorded in a STEM, which had a nominal resolution of only 0.42 nm. Here we examine the applicability of the same method to the imaging of zinc-blende semiconductor compounds. We discuss the conditions under which it is possible to resolve and identify the sublattices of the different constituents in the <110> orientation.

Ptychography

Hoppe proposed to perform a diffraction experiment with a coherent primary wave of suitable shape instead of plane wave illumination, which is used in conventional diffraction experiments. If we assume that the structure is a perfect crystal, for which the scattered waves are concentrated at discrete points in reciprocal space, then the philosophy behind the technique is to widen the reciprocal space points into regions which overlap. In the overlap region a phase sensitive addition of the beams of adjacent lattice points occurs. If the interaction of the specimen with the illumination is multiplicative, as in the case of a two-dimensional (infinitely flat) crystal, then the widening of the diffraction spots can be easily described as their convolution with the Fourier transform of the primary wavefunction which we call the aperture function. The advantage of this approach is that the interferences take place at the specimen level, from which the wave travels to the detector without further manipulation. In contrast to holography where the phase information is supplied through the interference of the scattered waves with a single reference wave which might have travelled a considerably different path length through the optical system, the basis of the approach outlined here is the reinterference of neighboring beams.

Ptychography is a general technique which in principle could be performed with all types of radiation, but the requirement of a high degree of coherence favors electrons over all other types of radiation because field-emission guns can produce electron beams of suitable brightness and coherence. Furthermore, electrons, being charged particles, can be easily deflected by magnetic and electric field configurations. In fact, modern high-resolution electron microscopes equipped with field-emission guns are ideally suited for the ptychographical technique, as they routinely produce electron probes with diameters below one nanometer. We will follow the nomenclature of the STEM where we can record coherent microdiffraction patterns consisting of coherently overlapping diffraction discs in the so-called microdiffraction plane. Hoppe suggested to use only one or two such patterns. Indeed, one pattern alone may contain enough information for a successful phase assignment if the examined structure consists of a two-dimensional lattice of a suitable geometry. Generally, one encounters a phase ambiguity, which is most easily resolved if either the beam is defocused - leading to straight fringes perpendicular to the disc separation vector as experimentally observed by Vine *et al.* (1992), Steeds *et al.* (1992), Vincent *et al.* (1993), Tanaka *et al.* (1994) - or if a series of patterns are recorded. Figure 1 shows calculated microdiffraction patterns for different probe positions both close to focus and with a large amount of defocus. The variation of the intensity distribution in the overlap regions depends on the direction of the probe movement with respect to the disc separation vectors. In Figure 1 the probe is moved in a direction indicated by the arrow and it is noticeable that there are interference regions in which the intensity distribution does not change. In the following, we will examine a four-dimensional data set of microdiffraction patterns $|M(\underline{\mu}', \underline{\rho})|^2$ recorded as a function of the probe position $\underline{\rho}$. In this notation reciprocal space coordinates are denoted by a dash, $\underline{\mu}'$ being a two-dimensional vector describing a position in the microdiffraction plane (i.e., a certain scattering angle) and $\underline{\rho}$ being a two-dimensional vector describing the position of the probe in the specimen plane. In the case of a perfect crystal, the probe movement gives rise to a sinusoidal intensity variation in the interference regions, and it is the phase of this intensity variation which we interpret as the phase difference between the diffraction orders. After the Fourier transformation of the data set with respect to the probe position interference regions as those depicted in Figure 2 show up for different spatial frequencies corresponding to different disc separation vectors. They yield the phase information which allows us to reconstruct the diffracted beams in amplitude and phase. For non-crystalline materials, applying a super-resolution algorithm (Rodenburg and Bates, 1992) to the four-dimensional microdiffraction data-set $|M(\underline{\mu}',\underline{\rho})|^2$ allows for the reconstruction of the wavefunction in amplitude and phase beyond the spatial frequency cut-off as defined by the aperture of the probe-forming lens.

Let us express the intensity distribution in the microdiffraction plane mathematically. If we assume that the illuminating aperture is fully coherently filled and that the interaction of the electron wave with the specimen is multiplicative, then the wave function in the microdiffraction plane is a convolution of the specimen function $\Psi(\underline{a}')$ with the aperture function $A(\underline{a}')$ in reciprocal space such that the intensity distribution is given by

$$|M(\underline{\mu}',\underline{\rho})|^2 = \iint A(\underline{\mu}'-\underline{a}')\, A^*(\underline{\mu}'-\underline{b}')\, \Psi(\underline{a}')\, \Psi^*(\underline{b}') \exp[2\pi i \underline{\rho}(\underline{b}'-\underline{a}')]\, d\underline{a}' d\underline{b}' \tag{1}$$

When the size of the objective aperture is such that the diffraction discs have just single overlap, the intensity in the overlap region between the disc **G** and **G**+**H** can be easily shown to be

$$|M(\underline{\mu}',\underline{\rho})|^2 = |\Psi_{\mathbf{G}}|2 + |\Psi_{\mathbf{G+H}}|^2 + 2|\Psi_{\mathbf{G}}|\,|\Psi_{\mathbf{G+H}}| \cos[(\alpha_{\mathbf{G+H}} - \alpha_{\mathbf{G}}) + (\chi(\underline{\mu}'-(\mathbf{G}+\mathbf{H})) - \chi(\underline{\mu}'-\mathbf{G})) + 2\pi\underline{\rho}\mathbf{H}] \tag{2}$$

where $\alpha_{\mathbf{G}}$ and $\alpha_{\mathbf{G+H}}$ are the phases of the beams **G** and **G**+**H**, respectively. The lens aberrations are expressed by the

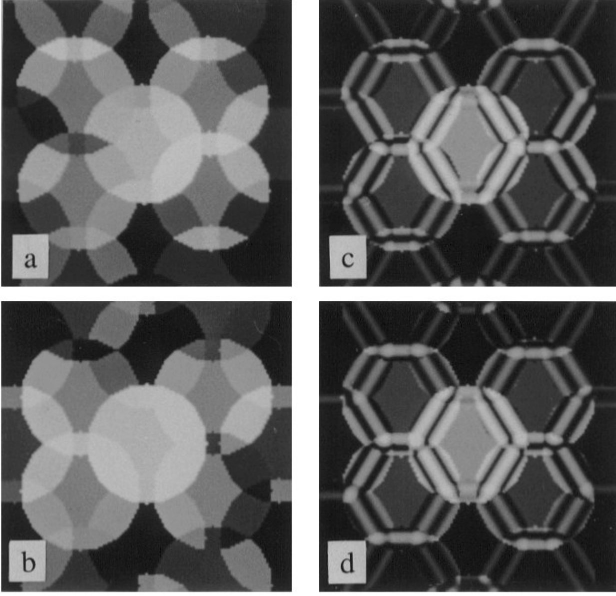

Figure 1. Calculated microdiffraction patterns for different probe positions: (**a**), (**b**) close to focus; (**c**), (**d**) with a large amount of defocus. The variation of the intensity distribution in the overlap regions depends on the direction of the probe movement with respect to the disc separation vectors. Here the probe is moved in a direction indicated by the arrow. There are interference regions in which the intensity distribution does not change.

function $\chi(\underline{a}')$, which is related to the aperture function $A(\underline{a}')$ by $A(\underline{a}') = |A(\underline{a}')| \exp(i\chi(\underline{a}'))$. The intensity in the overlap region is seen to vary sinusoidally as the probe is scanned parallel to the disc separation vector **H**. After taking the Fourier transform with respect to $\underline{\rho}$, $G(\underline{\mu}', \underline{\rho}')$ has considerable magnitude only for values of $\underline{\mu}'$ within the overlap region between the two discs when $\underline{\rho}'$ is equal to **H** or -**H**. For $\underline{\rho}'$ = **H** we have

$$G(\underline{\mu}', \underline{\rho}') = |\Psi_G|\,|\Psi_{G+H}| \exp[i(\alpha_{G+H} - \alpha_G) + \{\chi(\underline{\mu}'-(\mathbf{G}+\mathbf{H})) - \chi(\underline{\mu}'-\mathbf{G})\}] \quad (3)$$

The magnitude of $G(\underline{\mu}', \underline{\rho}')$ is given by the amplitude product of the reinterfering beams and its phase by their phase difference (including the aberrations introduced by the lens). For the measurement of the phase we shall extract the information from the point midway between the discs, i.e., from the centre of the interference regions, for which $\underline{\mu}'$ = **G**+**H**/2. In this point the two terms representing the lens aberrations in Equation (3) cancel if the aperture function is centro-symmetric. All the relative phases determined in this way are insensitive to lens characteristics (McCallum and Rodenburg, 1993). Using reconstruction methods as those discussed in the next section the Fourier space wave function can be retrieved, which via a Fourier transform yields a reconstructed real-space wave function in amplitude and phase.

Simple Reconstruction Methods

In the simple case of a perfect crystal of unit cell dimensions such that the discs in the microdiffraction plane just partly overlap as in Figures 1 and 2, all the diffraction discs can be successively phased (Spence and Cowley, 1978; Spence 1977, 1978). Such a reconstruction method - which we will refer to as reconstruction method I (RM I) - is allowed if the discs appear uniform, in which case the wavefield in the microdiffraction plane can be described as a convolution of the diffraction peaks of the specimen function with an aperture function - a characteristic which lent its name to the technique (πτυξ means 'fold'). In other words, the interaction of the electron probe with the specimen should be multiplicative. This is only valid in the case of a very thin but not necessarily only kinematically scattering crystal (e.g., when the phase object approximation holds) or in the limit as the wavelength of the scattering radiation tends to zero. For a finite wavelength amplitudes and phases of the scattered wave will vary across the disc diameter, when the crystal thickness exceeds a certain value. Broeckx *et al.* (1995) have related the assumption of a multiplicative interaction to the channelling of the STEM probe. In a forthcoming publication we will discuss the problems with the description of ptychography using dynamical diffraction theory in more detail.

Another simple approach to reconstruct the object wave function becomes apparent if we increase the radius of the aperture such that there is overlap between several diffraction orders and we consider the intensity variation midway in the overlap between the central disc and each diffracted disc. After Fourier transformation with respect to the probe position we obtain interference regions of the form depicted in Figure 3 for the case of the <110> zone-axis of a zinc-blende structure. In the reconstruction method discussed in the following, amplitudes and phases of the

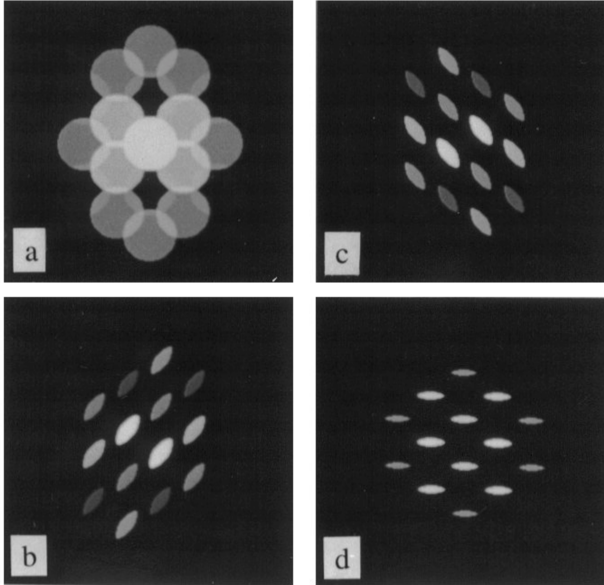

Figure 2. Interference regions which show up after Fourier transformation of the super-resolution data set with respect to the probe position for different spatial frequencies $\underline{\rho}'$: (**a**) $\underline{\rho}' = 0$; this is the sum of all patterns and corresponds to the incoherent convergent beam electron diffraction (CBED) pattern; (**b**, **c**, **d**) finite $\underline{\rho}'$, corresponding to different disc separation vectors and containing the phase information.

reconstructed beams are taken from the centre of the overlap between the central disc and the pertinent diffracted disc (these points are indicated by arrows in Figure 3). We shall refer to this approach as reconstruction method II (RM II). In the case of a strongly-scattering crystal we have to ensure that the centre of overlap between the central disc and each diffracted disc does not coincide with any part of the overlap region of two other discs, as this would lead to mixing of the interference regions. However, as Figure 3 indicates, we can find an aperture size for which the centers of all interference regions are not obscured. In particular, the two pictures on the right of Figure 3 correspond to the (002) and (004) reflections, respectively. We can conclude that for a suitable geometry of the diffraction pattern amplitude and phase of the reflections of the types **G** and 2**G** can be obtained, even if the overlap of the reflection 2**G** inevitably overlaps with the disc of the reflection **G**. If the aperture size was increased even further in Figure 3, then reflections higher than (004) could be reconstructed, but the method would break down for the low-order reflections (in this case the (111) reflection). It should be noted that points midway the central disc and the different diffraction discs, which are indicated by arrows, correspond to the Bragg condition for each beam. In the kinematical theory, it can be shown that the reconstructed wave function corresponds to a perfect projection of the specimen structure (Plamann and Rodenburg, 1994). It should be noted that the requirements on the degree of coherence in the illuminating electron beam is different for the two reconstruction methods. While it is only necessary that neighboring discs interfere coherently in RM I, the coherence in RM II must be sufficient to ensure detectable interference between the central disc and the highest-order disc which we want to phase.

We want to investigate the applicability of the two reconstruction methods, and we discuss the case of InP in the <110> orientation as an example below. The choice of this structure is motivated by recent, yet to be published work which demonstrated that the atomic columns of gallium phosphide can be clearly reconstructed using RM I. The reconstruction of the phase showed an excellent match with the projected structure. Direct resolution of the atomic columns along the <111> and <100> direction is more straightforward given their greater projected separation distance and the presence of a centre of inversion in these orientations (Ourmazd *et al*., 1986; see Kawasaki and Tonomura (1992) for reconstructions of InP <100> using holography). It should be noted that for a satisfying structural analysis of these materials, we require the ability not only to resolve the atomic columns but also to identify the atomic species occupying a given column. This is important for defect analysis, as defects in different sublattices show different mechanical and electronic properties.

Simulation Method

If we wanted to simulate the probe propagation through the crystal for each probe position, then we would have to make great demands on the size and the sampling of the used supercell. The computer time required would be proportional to $N_\mu'^2 N_\rho'^2 \log N_\mu'$, where N_μ' is the number of sampling points in the microdiffraction plane (that is, number of beams included in the calculation) and N_ρ' the number of probe positions. This would be identical to the simulation of annular dark field (ADF) images (Kirkland *et al*., 1987), which is notoriously slow. However, the propagation of the probe does not have to be calculated, at least not in the case of a perfect crystal, because the phase determination relies on the interference of only two beams from opposite points in the illuminating convergent beam. These beams propagate through the crystal independently of all other scattered beams and can thus be modelled by (tilted) plane wave illumination conditions in ordinary multi-slice programs. In the case of aperiodic specimens mixing of all the beams in the scattering process occurs and the full propagation of the probe has to be simulated.

Multi-slice simulations were carried out using the

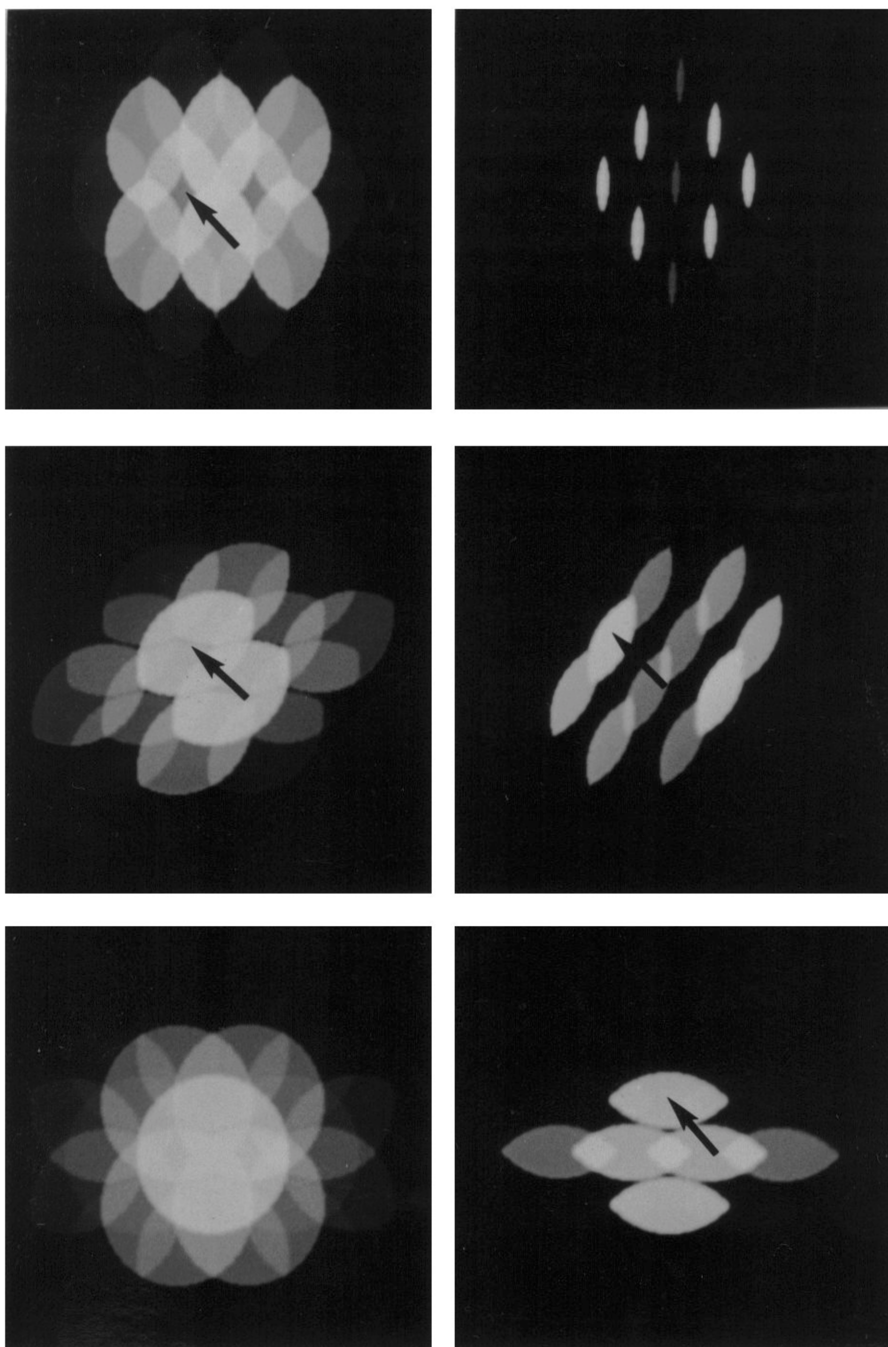

Figure 3. Interference regions for the case of a bigger aperture; in reconstruction method II amplitudes and phases of the reconstructed beams are taken from the centre of the overlap between the central disc and the pertinent diffracted disc, indicated by arrows.

Figure 4 (*on next two pages*). Comparison of different reconstruction methods on InP <110>.

software package CERIUS (developed by Molecular Simulations, Cambridge, UK). The electron scattering factors of Doyle and Turner (1968) were used, and Debye Waller factors were taken from Reid (1983). Illumination tilts $\mathbf{K}_t$ of the incoming plane wave were modelled by the alteration of the propagation function P(**K**) in Fourier space according to:

$$P(\mathbf{K}) = \exp \pi i \lambda \Delta z (\mathbf{K}+\mathbf{K}_t)^2 \quad (4)$$

which corresponds to a slight shear of the specimen such that every successive slice is shifted by a small amount (Self *et al.*, 1983).

In contrast to conventional lattice imaging we do not have to calculate the effect of the lens aberrations on the lattice interference fringes, as we always choose diffraction information from the centre of overlap between the discs, which is not affected by the lens transfer function, provided that the objective lens is perfectly aligned (see

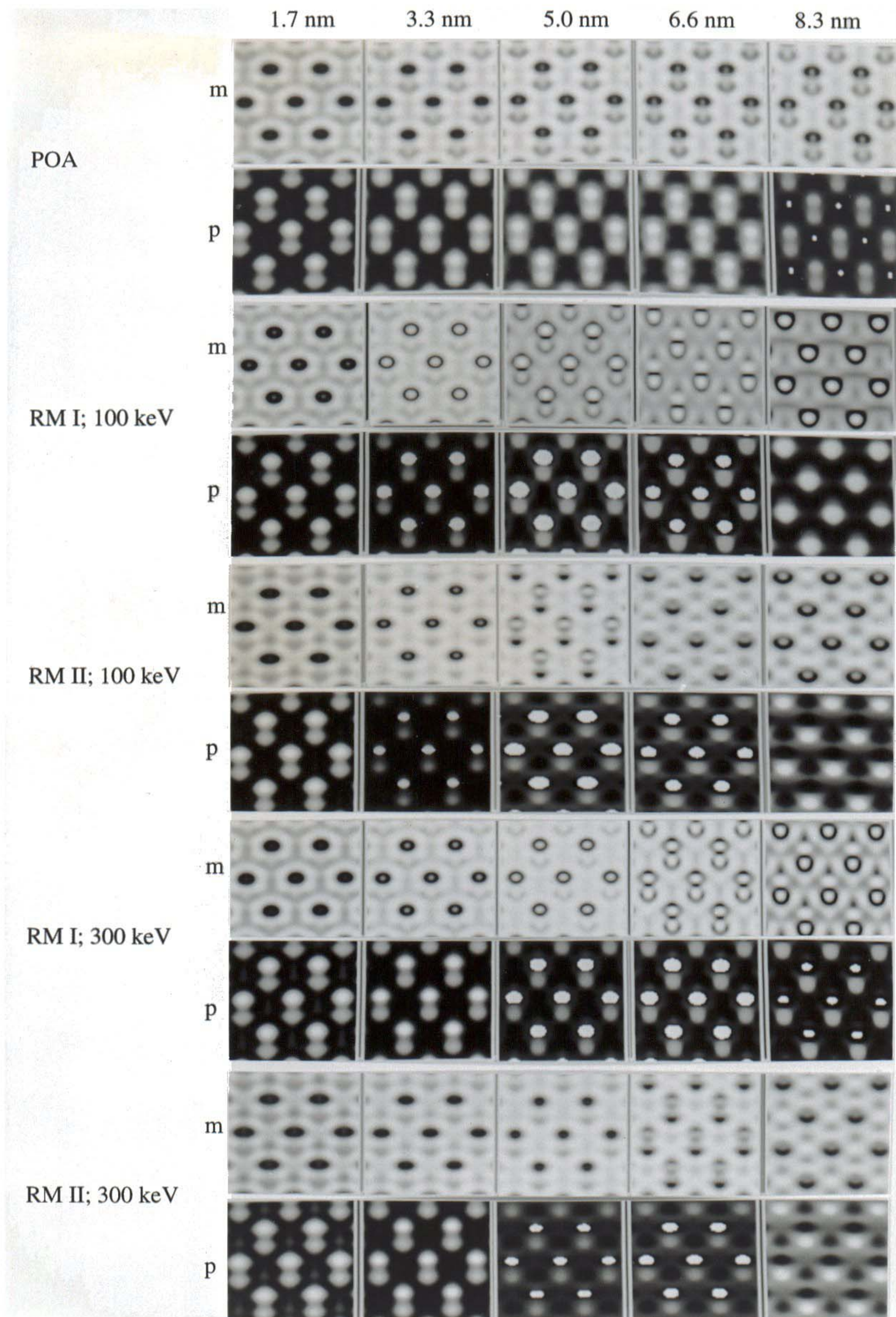
1.7 nm
3.3 nm
5.0 nm
6.6 nm
8.3 nm
POA
m
p
RM I; 100 keV
m
p
RM II; 100 keV
m
p
RM I; 300 keV
m
p
RM II; 300 keV
m
p

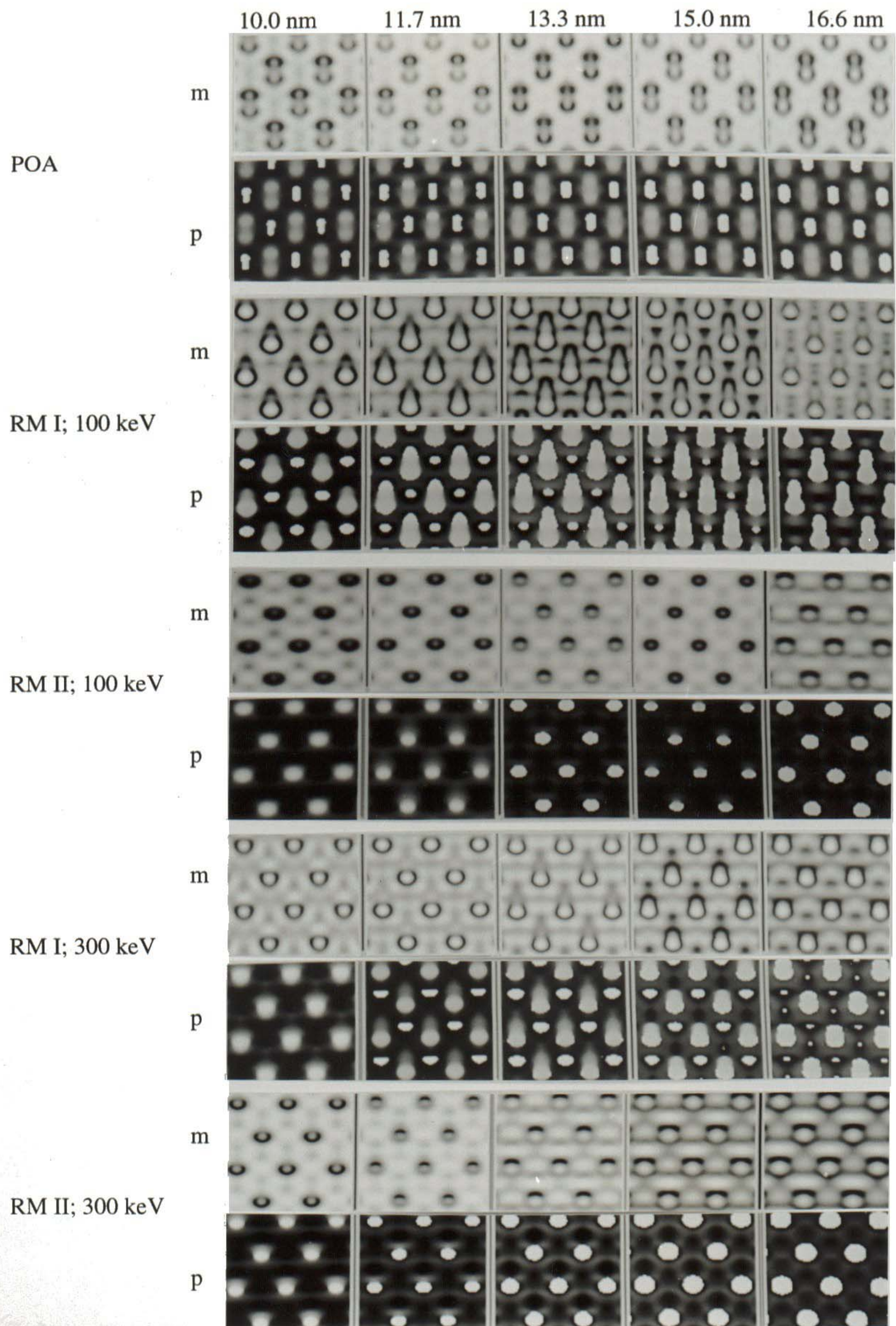
10.0 nm
11.7 nm
13.3 nm
15.0 nm
16.6 nm
POA
m
p
RM I; 100 keV
m
p
RM II; 100 keV
m
p
RM I; 300 keV
m
p
RM II; 300 keV
m
p

above). Hence, the defocus is not a free parameter in the calculations.

Simulations on InP <110>

We introduced two different reconstructions methods above. In Plamann and Rodenburg (1997) it is shown that the reconstructed object wave functions do not correspond to the exit surface wave functions (ESWFs) obtained under axial illumination conditions, but to 'backpropagated' wave functions pertaining to the middle section of the crystal. These functions are somewhat closer to pure phase objects than the ESWFs. In the following, we will make a comprehensive comparison between the different reconstruction methods for two accelerating voltages with the strict phase object approximation (POA), using InP <110> as an example. The examination of the thickness limitations of the different reconstruction methods is important for the determination of instrumental parameters such as accelerating voltage or coherence width which are most suited for the performance of super-resolution experiments.

In each case (RM I, RM II and POA) the object wave function was calculated in Fourier space, yielding the complex values of the 19 innermost beams. Then a Fourier transform was taken to obtain a periodic function in real space. It is obvious that if we multiply the wave functions by a constant phase, we obtain another possible solution. We assigned a phase of -2.5 rad to the central beam in order to avoid a phase wrap-around on the indium column for small thicknesses. The object wave functions in Fourier space were calculated as follows:

RM I: First, we calculated amplitudes of all beams including the {004} reflections for axial illumination, that is $\mathbf{K}_t = 0$. This produced the beam amplitudes for the ptychographical reconstruction which are extracted from the centers of the diffraction discs. Second, we calculated phase differences between pertinent beams by applying tilted plane wave illumination conditions. All beams were phased successively, using the shortest routes available.

RM II: For the reconstruction of each Fourier component of the reconstructed wave function, each beam was set into the Bragg condition, successively. The amplitude of the reconstructed Fourier component was set to the calculated amplitude product of the central beam and the pertinent beam, and its phase was set to the calculated relative phase. The amplitude of the central beam in the reconstruction was set to unity.

POA: In the POA the potential distribution is projected onto a two-dimensional surface. The thickness values in Figure 4 do not correspond to an actual distance, but to the scaling factors of the projected potential. In the calculation, the propagation between successive slices was neglected. Phase transmission functions were calculated at an accelerating voltage of 100 keV. The propagator in Equation (4) was set to unity. It is apparent that no illumination tilts had to be modelled, since in the POA the beam amplitudes are the same for each illumination tilt.

Figure 4 shows the magnitude (m) and phase (p) components of our reconstructions at thickness steps of 1.7 nm. For t = 1.7 nm the image features in the five rows look somewhat similar. This is expected because at small thicknesses the POA can be made. However, even at a thickness as small as 3.3 nm the images start to look considerably different: While for 300 keV the reconstructed phase for both reconstruction methods matches the phase in the POA, the indium column shows up much stronger in the phase of the reconstructions for 100 keV, since the POA breaks down more rapidly for smaller accelerating voltages. At slightly larger thicknesses (5.0 - 6.6 nm) the phase of the reconstructions consistently shows a close resemblance to the projected structure, with a greater phase shift on the upper indium column and a clear expression of the crystal polarity. In contrast to the phase, the magnitude components of the reconstructions do not match the structure reliably. We note that there is an apparent inversion of the dumbbell asymmetry in the magnitude component between 5 and 6.6 nm for RM I at 100 keV. Surprisingly, the “dumbbells” look almost symmetrical in the phase of the POA. This is a consequence of the truncation of the wave function in Fourier space. For a perfect phase object the indium column scatters into higher diffraction orders which are not included in the wave function shown here. If the POA wave function comprised more beams, the asymmetry would become more apparent.

At thicknesses exceeding 8.3 nm the image reconstructions break down successively and do not show the atomic positions reliably. The first reconstruction method to break down is RM I at 100 keV (for RM II at both accelerating voltages and t = 8.3 nm the indium column appears dark as a consequence of a phase wrap-around), but all the others follow quickly. The images at these larger thicknesses cannot be called structure images. However, let us consider the phases of the RM II wave functions for thicknesses greater than 10 nm. They all show strong bright patches on top of the phosphorus column, while the indium column is not visible except for the case of 300 keV, in which it shortly re-appears at 13.3 nm. The striking appearance of the phosphorus column in the reconstructions is not yet understood. The dynamical scattering for RM II is rather complicated, since all beams are brought into the Bragg condition, successively. However, the reason for the dominance of the phosphorus column has probably to do with the strong excitation of its s-states. The result also seems to be in agreement with simulations of annular dark-field images of InP (Hillyard *et al*., 1993), in which the channelling peak on top of the indium columns was shown

to disappear at thicknesses around 10 nm.

Conclusions

Simulations on InP <110> for two electron accelerating voltages have shown that the asymmetric "dumbbells" can be reconstructed for small thicknesses below 8 nm. In this thickness regime the choice of the reconstruction methods and of the accelerating voltage does not make any significant difference. This is an essential result as the experiments can be performed at relatively low voltages and with only modest coherence. It was shown that at larger thicknesses the reconstruction method which requires a high degree of coherence yields images which show the phosphorus columns very clearly and partly also the indium columns, though very weakly.

References

Broeckx J, Op de Beeck M, Van Dyck D (1995) A useful approximation of the exitwave function in coherent STEM. Ultramicroscopy **60**: 71-80.

Coene W, Janssen G, Op de Beeck M, Van Dyck D (1992) Phase retrieval through focus variation for ultra-resolution in field-emission transmission electron microscopy. Phys Rev Lett **69**: 3743-3746.

Doyle PA, Turner PS (1968) Relativistic Hartree-Fock X-ray and electron scattering factors Acta Cryst **A24**: 390-397.

Hillyard S, Loane RF, Silcox J (1993) Annular dark-field imaging: resolution and thickness effects. Ultramicroscopy **49**: 14-25.

Hoppe W (1969a) Beugung im Inhomogenen Primärstrahlwellenfeld. I. Prinzip einer Phasenmessung von Elektronenbeugungsinterferenzen (Diffraction in an inhomogenous primary beam wavefield. I. Principle of a phase measurement by electron diffraction interference). Acta Cryst **A25**: 495-501.

Hoppe W (1969b) Beugung im Inhomogenen Primärstrahlwellenfeld. III. Amplituden- und Phasenbestimmung bei unperiodischen Objekten. (Diffraction in an inhomogenous primary beam wavefield. III. Determination of amplitudes and phases in non-periodic objects). Acta Cryst **A25**: 508-514.

Hoppe W (1982) Trace structure analysis, ptychography, phase tomography. Ultramicroscopy **10**: 187-198.

Kawasaki T, Tonomura A (1992) Direct observation of InP projected potential using high-resolution electron holography. Phys Rev Lett **69**: 293-296.

Kirkland AI, Saxton WO, Chau K-L, Tsuno K, Kawasaki M (1995) Superresolution by aperture synthesis: tilt series reconstruction. Ultramicroscopy **57**: 355-*last page*.

Kirkland EJ, Loane RF, Silcox J (1987) Simulation of annular dark field images using a modified multislice method. Ultramicroscopy **23**: 77-96.

Lichte H (1992) Electron Holography. I. Can electron holography reach 0.1 nm resolution? Ultramicroscopy **47**: 223-230.

McCallum BC, Rodenburg JM (1993) Error analysis of crystalline ptychography in the STEM mode. Ultramicroscopy **52**: 85-99.

Nellist PD, McCallum BC, Rodenburg JM (1995) Resolution beyond the "information limit" in transmission electron microscopy. Nature **374**: 630-632.

Ourmazd A, Rentschler JR, Taylor DW (1986) Direct resolution and identification of the sublattices in compound semiconductors by high-resolution transmission electron microscopy. Phys Rev Lett **57**: 3073-76.

Plamann T, Rodenburg J M (1994) Double resolution imaging with infinite depth of focus in single lens scanning microscopy. Optik **96**: 31-36.

Plamann T, Rodenburg J M (1998) Electron ptychography II: Theory of three-dimensional propagation effects. Acta Cryst **A54**: 61-73.

Reid J (1983) Debye-Waller Factors of zinc-blende-structure materials - a lattice dynamical comparison. Acta Cryst **A39**: 1-13.

Rodenburg JM, Bates RHT (1992) The theory of super-resolution electron microscopy via Wigner-distribution deconvolution. Phil Trans Roy Soc Lond **A339**: 521-553.

Self PG, O'Keefe MA, Buseck PR, Spargo AEC (1983) Practical computation of amplitudes and phases in electron diffraction. Ultramicroscopy **11**: 35-47.

Spence JCH (1977) Phase determination of multiply scattered beams in STEM. Optik **49**: 117-120.

Spence JCH (1978) Practical phase determination of inner dynamical reflections in STEM. Scanning Electron Microsc 1978; I: 61-68.

Spence JCH, Cowley JM (1978) Lattice imaging in STEM. Optik **50**: 129-142.

Steeds JW, Vincent R, Vine WJ, Spellward P, Cherns D (1992) Exploratory experiments in convergent beam coherent electron diffraction. Acta Microsc **1**: 1-13.

Tanaka M, Terauchi M, Tsuda K (1994) Convergent-beam electron diffraction III. Jeol Ltd., Tokyo.

Van Dyck D, Op de Beeck M, Coene W (1993) A new approach to object wavefunction reconstruction in electron microscopy. Optik **93:** 103-107.

Vincent R, Vine WJ, Midgley PA, Spellward P, Steeds JW (1993) Coherent overlapping LACBED patterns in 6H SiC. Ultramicroscopy **50:** 365-376.

Vine WJ, Vincent R, Spellward P, Steeds JW (1992) Observation of phase contrast in convergent-beam electron diffraction patterns. Ultramicroscopy **41**: 423-428.

Discussion with Reviewers

P.W. Hawkes: In the comments on coherence, I think that spatial coherence (corresponding to source size) is meant. How will the conclusions be affected by temporal coherence?
Author: The effects of temporal coherence can be thought of as a rapid variation of defocus. In the midpoint of the overlap region between two diffraction discs, in which the phase is measured, the defocus term cancels as well as all other centro-symmetric terms of the aperture function [see Equation (4) for $\underline{\mu}' = \mathbf{G}+\mathbf{H}/2$]. As a consequence, temporal coherence does not affect the measured phase, as long as the pixel size of the detector is chosen fine enough.

P.W. Hawkes: What specimens will be studied in the next stage of the project?
Author: Previous experiments on silicon and gallium phosphide have been very successful. It would now be very interesting to apply the technique to materials with large unit cells. It is clear that for a given reflection, several routes can now be taken to determine its phase. The redundancy in phase information should give a means of reducing the error of the phase estimate.

R. Hegerl: Following the original ideas of W. Hoppe, ptychography should be applied to two-dimensional crystals of biological macromolecules. Apart from the much larger lattice periods, problems may arise from the need of a low electron dose and the resulting low signal-to-noise ratio. Assuming a tolerable electron dose of say 1000 el/nm^2 (summed over all exposures of the specimen area), is there a chance to obtain reliable phase information?
Author: The applicability of ptychography to biological specimens has yet to await experimental evidence. However, it is worth considering the effect of the sampling of the probe position. When we record our four-dimensional data set of microdiffraction patterns $|M(\underline{\mu}', \underline{\rho})|^2$ as a function of the probe position $\underline{\rho}$, we have to ensure that all the probe positions are equi-distant, but the distance between them can be chosen quite freely. The aim would be to choose the distance as great as possible. That reduces the effect of specimen damage. However, one has to make sure that the thickness and orientation of the crystal does not change too much across the pertaining area. Furthermore, the number of probe positions required may be quite small. On the other hand, one would probably use neither of the reconstruction methods described above, in which only certain points of the microdiffraction plane are considered. In order to account for every electron contained in the data-set, a deconvolution as described in Rodenburg and Bates (1992) could be favorable.